A machine learning approach to address the issue of false positives and false negatives in active structural health monitoring (SHM)

Kranthi Kode, Fatih Sunor & Surajit Roy

December 12, 2010

Abstract:

This study proposes distinct new features in the PZT sensor signals to separate the effects of damage (edge cracks) and non-damage (temperature and applied loads) conditions in the metallic structures. Experiments conducted on thin rectangular aluminum specimens show that the specific combination of signal feature and machine learning algorithm can reduce the false negatives to less than 12%, while the false positives lie well within 30%. The proposed methodology is also tested for scalability by applying the learning algorithm to different geometry and different damage type.

Introduction:

Active structural health monitoring (SHM) employs the concept of anomaly detection in a structure based on the propagation of lamb waves. These waves are generated using the principle of piezoelectricity by piezoceramic (PZT) transducers. The PZT sensor signals, representing the propagation of lamb waves, may undergo change in their characteristics (phase, amplitude or spectral content) while propagating through the structure. These changes can either be caused by intrinsic factors such as fatigue cracks, surface corrosion, delaminations or extrinsic factors such as changes in environmental temperature, changes in loading and boundary conditions. The key challenge in the SHM is to address the problem of false-positives, wherein the system mistakenly attributes the changes in the operational and environmental conditions to the presence of defects inside the material. The objective of this study is to develop a classification model based on the machine learning approach that can reduce the problem of false positives and false negatives to a considerable extent.

Experimental Setup:

In this study, the signals representing the propagation of lamb waves in a structure are generated and collected from two separate 'smart layers' attached on the surface of the test coupons. Each 'smart layer' has four PZT transducers, which can act as both actuators and sensors. The signals are generated in a pulse-echo mode where one 'smart layer' sends the excitation pulse while the other one records the received waveform. The basic experimental setup for static loading and the test coupon with attached 'smart layers' are shown in Fig. 1.

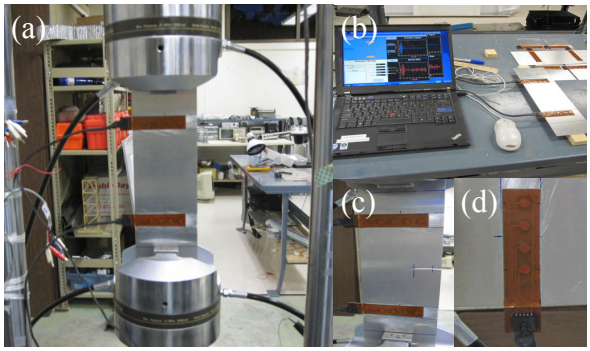

Figure 1: (a) Test coupon subjected to loading in MTS machine (b) Data acquisition System (c) Coupon with induced damage (1½" straight edge crack) at the center and (d) 4-PZT sensor strip 'smart layer' attached to the test coupon

The test coupons are thin rectangular aluminum ('Al 6065 alloy') plates having dimensions as 14"x4.5"x0.078". The present study is carried out with 'Burst3' (3-peaks Gaussian tone-burst) signal type at an actuation frequency of 250 kHz. The choice of signal parameters is governed by the clear resolution of the signal in both the time and frequency domain. The effect

of temperature, load and damage on one of the sensor signals is shown in fig. 2.

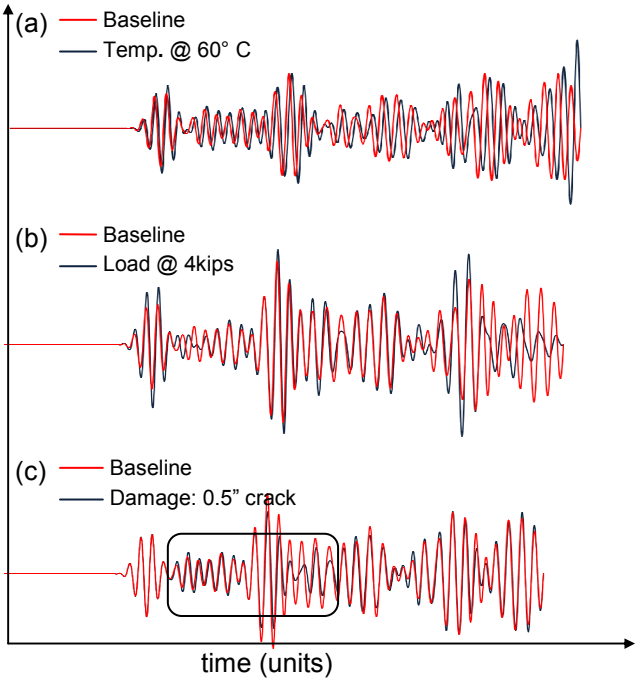

Figure 2: Effect of (a) Temperature, (b) Load and (c) Damage on a specific PZT sensor signal. The box in figure (c) highlights the localized changes in the signal in the time domain whereas for figures (a) and (b) the changes w.r.t the baseline signal can be observed in the entire time domain.

The PZT sensor signals are collected from the test coupons at different levels of elevated temperatures, static loads and induced damages. The temperature data ranging from 30ºC to 90ºC is collected in a controlled environmental chamber. The static load data is collected by loading the test coupons in MTS machine and recording the data at different load levels. The experiments are repeated thrice for consistency in data collection. The damage conditions are simulated by introducing edge cracks of varying lengths on the coupons at different locations. The training data for the damage condition is collected from the coupons with straight edged cracks at the center of the specimen. The damage data corresponding to the test set is obtained from coupon with cracks starting at different location and propagating along different direction as shown in fig. 3.

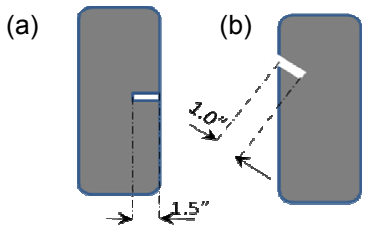

Figure 3: (a) Coupon layout: Training set, straight edge cracks starting at the center; (b) Coupon layout: Test set, cracks starting at different location and propagating along different direction

Methodology:

The data collected at elevated temperatures and at different load levels are classified as 'non-damaged' data whereas the rest of the signals are considered as 'damaged data'. The training set has 560 'non-damaged' and 128 'damaged signals' whereas the test set has 208 'non-damaged' and 128 'damaged' signals. New and unique features from the signal data are identified based on the hypothesis that damaged conditions will cause only localized changes in the signal in time domain and vice-versa for non-damaged conditions. The performance measures for each of these features are studied with different classification algorithms to select only a few set of features. This subset of features along with the best classification algorithms are finally tested on new geometry and new damage type for the scalability and baseline transfer approach.

Feature Selection:

The following sets of features are identified based on the aforementioned hypothesis.

Feature I) & II) Signal Scatter Amplitudes: The feature type I and type II consists of the whole and sub-section of scatter signals respectively. Scatter signal is the difference between the recorded sensor signals under different experimental conditions and the baseline sensor signals, representing the pristine and undamaged state of the structure.

Feature Type III), IV), V), VI) & VII) Uniformly Discretized Signal Vector: The signal data is discretized into uniformly spaced intervals (bins) in the time domain. Each bin is assigned with a characteristic number based on the behavior of the signal at different time intervals. Feature type III is the norm of the scatter signal within each bin. Feature type IV is the maximum of peak to peak amplitude difference between the sensor signals, collected at different experimental conditions, and the corresponding baseline signals within each bin (shown in fig. 4). Feature type V is the maximum phase shift between the peaks of the sensor signals and the corresponding baseline signals within each bin respectively.

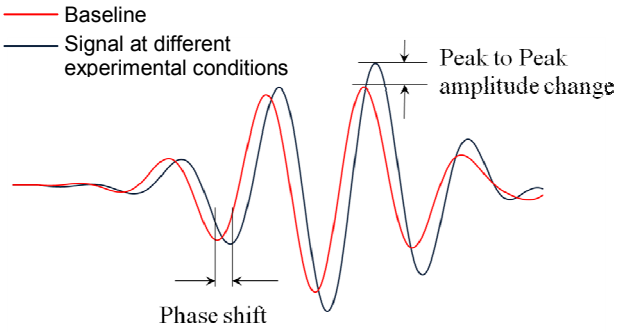

Figure 4: Peak to peak amplitude change and phase shift between the baseline signal and signals collected at different experimental conditions

Feature type VI is the combination of feature types IV and V whereas feature type VII is the combination of feature type IV and average of the phase shifts in each bin. Fig. 5 shows the effect of changing the number of bins on the prediction of 'false negatives' corresponding to the test set data. The optimal number of bins considered in this study is '25' based on the sensitivity analysis.

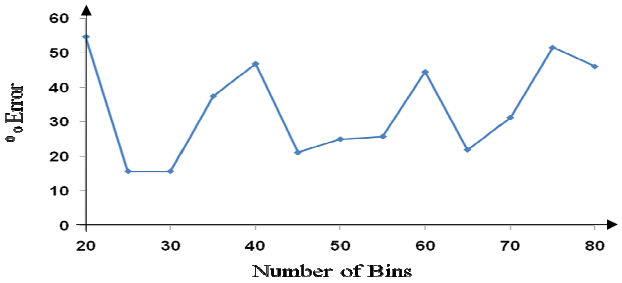

Figure 5: Plot of % error in classifying damage data ('false negatives') in the test set vs. number of bins of the signal vector.

Feature Type VIII) Singular values of STFT magnitudes 'time-frequency matrix': The time-frequency analysis of the scatter signal for a given actuator-sensor pair is carried out using the short-time Fourier transformation. It is hypothesized that the changes in the spectral content of the signal over the time may help in separating out the damage characteristics hidden in the signal from the non-damage characteristics. The spectral content of the scatter signal, STFT magnitude, is then decomposed using singular value decomposition (SVD) to obtain its lower rank approximation. Fig. 6 represents the percentage errors in classifying damage data in the test set with different number of singular values as the classifying feature.

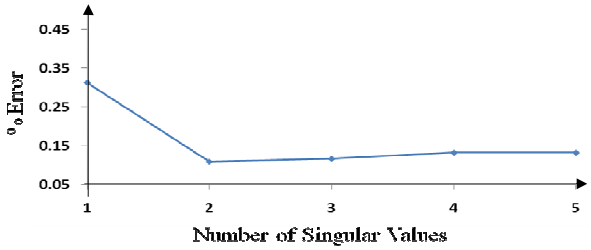

Figure 6: Plot of % error in classifying damage data ('false negatives') in the test set vs. number of singular values of STFT magnitude of the scatter signal vector.

Feature type VIII is the first three singular values of the spectral content of the scatter signal. The later singular values are relatively smaller and hence have lower significance for learning models as is shown in fig. 6.

Results:

Fig. 7 shows the plot of percentage errors in classifying damage vs. non-damage signals in the test set for different machine learning algorithms. The three different machine learning algorithms used in this study are 'Bayesian Logistic Regression' (BLR), 'Gaussian Discriminant Analysis' (GDA with different mean and covariance for the damage and non-damage sets) and 'Support Vector Machines' (SVM with linear regularized kernel). The parameters used in the 'BLR' and 'SVM' are

chosen such that their small variation does not affect the output of these algorithms.

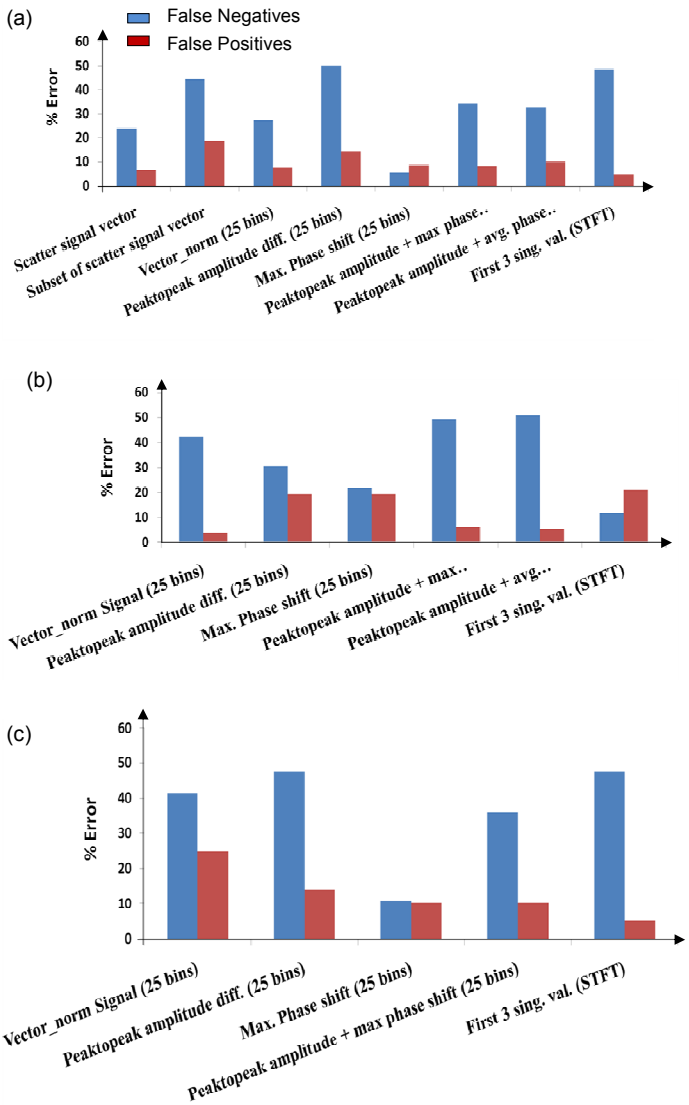

Figure 7: Plot of % errors in classifying the damage signals for test set data with different classification algorithms: (a) Support vector machines (linear regularized kernel), (b) GDA and (c) Bayesian Logistic Regression.

It can be seen from fig. 7 that the percentage error in classifying the non damage data (false-positives) is within 25% for all the features and for all the algorithms. The percentage errors in classifying the damaged signals ('false-negatives') are extremely high for almost all the features. It needs to be mentioned here that 'false negatives' should be as low as possible for the practical viability of any classification algorithm.

However there are specific feature and algorithm combinations where the 'false negatives' are at par or lower than the 'false positives'. The feature 'type V' (max phase shift (25 bins)) shows greater accuracy in classifying the damage vs. non-damage data for all the algorithms as compared to other features. Physically this behavior can be attributed to the type of damage we are observing in our train and test data. The edge cracks result in the phase delay of the damage signals occurring only at specific time of interest as shown in fig. 2c. The effect of discretizing the time and considering the maximum of the phase shifts in each bin as the feature vector enhances the probability of classifying this type of damage data. Additionally one more feature, type VIII, is identified which works well with 'GDA'. This feature (first three singular values of STFT) achieves classification between damage and non-damage signals within an error of 22%.

Figs. 8 (a) & 8 (b) shows the 'Precision-Recall' curves for feature 'type V' and 'type VIII' with different combination of classification algorithms. A comparison of area under the precision-recall curves for different features and different algorithms is also shown in fig. 8 (c). It can be inferred from figs. 7 and 8 that the best feature and classification algorithm combinations are i) Model 'A': feature 'type V' (max. phase shift (25 bins)) with 'SVM' and ii) Model 'B': feature 'type VIII' (first 3 singular values of STFT) with 'GDA'.

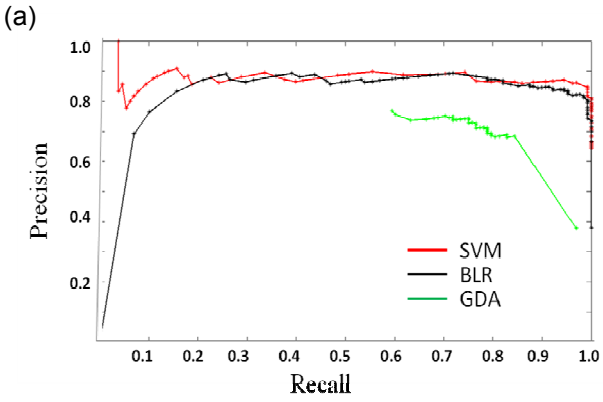

(b)

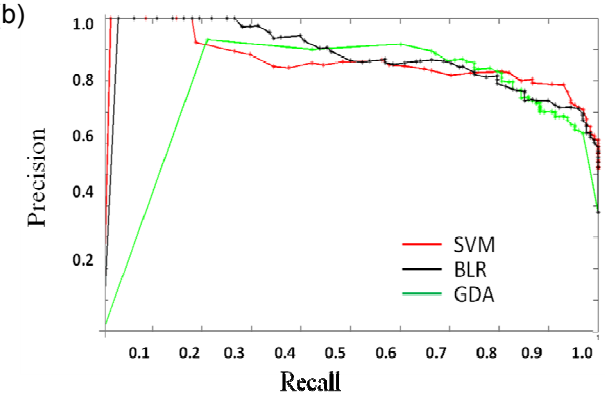

(c)

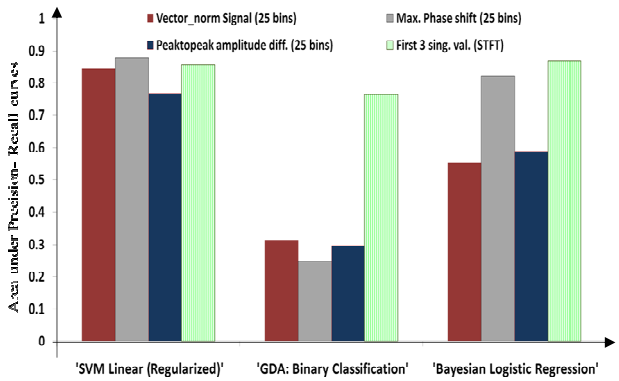

Figure 8: (a) Precision-Recall curve for feature 'type V' (max. phase shift (25 bins), (b) Precision-Recall curve for feature 'type VIII' (first 3 singular values of STFT) and (c) Area under the Precision-Recall curve for different features and different classification algorithms

Testing Scalability:

Table 1 summarizes the performance of best feature and algorithm combinations for different test cases. The study thus far has resulted in classification models that can classify between the damaged and non-damaged signals within an error bound of 30% in both the training and test set data. The model is then tested for scalability, wherein the signals collected on new geometry and new damage type, as shown in fig. 9, are classified as either damaged or non-damaged. Surprisingly the learning model 'B' tracks both the damaged and non-damaged signals quite accurately. The learning model 'A' however does not work with new damage type indicating that this feature is sensitive to the type of damages. Physically the drilled hole at the center is obstructing the direct path of the wave propagation from actuators to sensors. The prominent effect of this damage type is reduction in signal amplitudes without having significant contribution to the localized phase changes in the sensor signals.

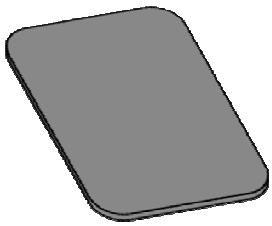

Figure 9: Test Case (a), Classification of Temperature data @ 60° C - Rectangular Plate 18"x12"x.078"

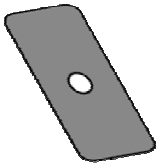

Figure 9: Test Case (b), Classification of new damage type - Drilled hole at the center

Table 1: Summary of performance of learning model 'A' and model 'B' on training and test sets

	Model 'A' (% error)		Model 'B' (% error)	
	False Positives	False Negatives	False Positives	False Negatives
Training Set	**2.6786**	**8.5938**	**29.4643**	**9.375**
Test Set	**8.6538**	**5.4688**	**21.1538**	**11.7188**
Test Case a.) New Geometry with temp. data only	**0**	---	**0**	---
Test Case b.) New Damage type	---	**75**	---	**0**

Conclusions:

The present study identifies best feature and learning algorithm combinations to classify the PZT sensor signals as 'damaged' or 'non-damaged' for metallic structures. The damage represented by edge cracks in metals can be classified with very high accuracy (low test and training set errors), however further investigation is required to make this method work for different type of damages.

References:

1.) Andrew Ng., CS229 Class Notes, 2010.

2.) Keith Worden and Graeme Manson, The application of machine learning to structural health monitoring, *Phil. Trans. R. Soc. A 2007 365, 515-537.*